Shahrood University of Technology

Journal of Mining and Environment (JME)

Journal homepage: www.jme.shahroodut.ac.ir

Iranian Society of Mining Engineering (IRSME)

Failure Mechanisms of Concrete-Bolt Attachment Surface: Impact of Cable Bolt Indent Number and Shape

Vahab Sarfarazi[1], Lei Zhou[2,3], Hadi Haeri[4*], Parastou Salehipour[5], Ali Elahi[4], Ali Moayer[6], Mohammad Fatehi Marji[7]

1. Department of Mining Engineering, Hamedan University of Technology, Hamedan, Iran
2. State Key Laboratory of Oil and Gas Reservoir Geology and Exploitation, Southwest Petroleum University, Chengdu , 610500, China,
3. State Key Laboratory of Intelligent Construction and Healthy Operation and Maintenance of Deep Underground Engineering, College of Architecture and Environment, Sichuan University, Chengdu 610065, China
4. Department of Mining Engineering, Higher Education Complex of Zarand, Shahid Bahonar University of Kerman, Kerman, Iran.
5. School of natural resources and the environment, West Virginia University, Morgantown, West Virginia, USA
6. Department of civil engineering, Islamic Azad University of Shiraz, Shiraz, Iran.
7. Department of Mine Exploitation Engineering, Faculty of Mining and metallurgy, Institute of Engineering, Yazd University, Yazd, Iran

Article Info

Received 18 April 2024
Received in Revised form 13 July 2024
Accepted 15 August 2024
Published online 15 August 2024

DOI: 10.22044/jme.2024.14440.2707

Keywords

Tensile strength
Rock bolt indent shape
Interface
Discrete element method

Abstract

The mechanical behavior of rock-rock bolt interface considering the effects of indents' shape and their number was numerically simulated based on discrete element method using the two-dimensional particle flow code. The conventional and standard uniaxial compressive and Brazilian tensile strengths tests were used to calibrate the modelled samples with 100 cm 100 cm in dimension. The numerical models were prepared such that different indent shape and number were inserted in the cable bolts arrangements during the rock reinforcement process. The effects of confining pressure 3.7 MPa and different shear failure loads were modeled for the punch shear test of the concrete specimens. The results of this study showed that the dominant failure mode of the rock-cable bolt interface was of tensile mode and the shape and number of cable indents significantly affected the strength and mechanical behavior of the modelled samples. It has also been showed that the indent dimensions and number affected the shear strength of the interfaces.

1.Introduction

One of the common ways in rock engineering to stabilize the ground and improving safety of working is using rock bolts [1]. There are different kinds of rock bolts, but two kinds of rock bolts including the fully bonded bolt and the prestressed bolt, due to their effectiveness and applicability, are mostly used in civil and mining engineering. Rock burst, generally, releases a great amount of energy [2-17] which usually causes serious damage to on-site construction and put the site workers of deep rock engineering in a serious danger. Due to these threats, in recent years, new generation of rock bolts, such as the cone bolt [7, 11,18-21], the Durbar [5], the D-bolt [8-10], and other energy-absorbing bolts [22,23], have been developed to solve the issue.

Designing a support in rock engineering requires a deep comprehension of the working mechanism and anchoring effect of rock bolts. Furthermore, in the past decades extensive research studies have been conducted to address this problem using theoretical analysis [24-26], laboratory experiments [27, 28], and numerical modeling [29-34]. Selvadurai and Yu [35], simulate the joint direct shear tests using the finite element method, and the simulated results were in good correlation with the experimental results. There are both advantages and disadvantages to using continuum mechanics theory for studying the failure and deformation mechanisms of jointed rock masses. The main disadvantages are that the effects of joints and rock

Corresponding author: haerihadi@gmail.com (H. Haeri)

weakening during the loading process especially at failure and breaking stages are not realistically determined. Therefore, the numerical simulation of the failure and fracture mechanism of jointed rock masses using different numerical technics are of the most important in rock engineering practice. The finite element, boundary element, finite difference and discrete element methods are the mostly used numerical modelling of geo-mechanical problems occurring in mining, tunnelling, civil, petroleum, geological and environmental engineering fields. The discrete element method (DEM) has been effectively used by many investigators to simulate the rock fracture mechanics problems. The particle flow code (PFC) which is based on the explicit finite difference approach considering different contacts and parallel joint surfaces is specially modified to solve many geo-mechanical problems involving joints and discontinuities in the rock structures of engineering projects. For example, the direct shear test was used by Zhou et al. [14] to study the failure and fracture process of jointed rocks considering the microscopic and macroscopic properties of the PFC models. The effects of microscopic and geometrical properties of rock joints on the shear and mechanical characteristics of rock masses was investigated by Park and Song [36], using a three-dimensional PFC (PFC3D). However, these researchers showed the applicability and effectiveness of using PFC as a powerful and reliable modelling techniques for the treatment of geo-mechanical and geo-technical problems. Simultaneously, many researchers worked on the numerical simulation of the jointed rock reinforcement through rock bolts. For instance, the interface and contact mechanics principles for jointed rocks can be simulated using PFC [18]. However, some continuous and coupling methods may give more consistence and realistic results for rock bolt mechanism of reinforcement. Rock bolts are considered as continuous and homogeneous media, for which finite element method (FEM) can be effectively used to model the mechanical behavior of bolts. On the other hand, the cohesive zone model (CZM) introduced by Dugdale [37] has been widely used for the simulation of cracked fragile materials. CZM-FEM can simulate the crack propagation process in brittle materials such as rocks and concretes. It has been shown that the crack propagation in composite plates and the bond-slip in the interaction surface between steel rebars and concrete can be described by CZM-FEM [38, 39]. Therefore, the crack initiation process in brittle material was simulated considering the crack tip singularity effects on the near field stress field. The CZM approach was extended by Su et al. [40], who used the solid grids in FEM and proposed a new algorithm for including the cohesive elements in the discretization scheme of complex structures posing to fracture and collapse. In this research, the effects of cable bolt indent shape and its number on the mechanical and sliding behavior of the interface between the rock and rock bolt are studied numerically using the two-dimensional PFC. Failure pattern, failure mode and bearing capacity of cable were studied, too.

1.1. Bonded particle models

The two-dimensional PFC [41] is used as the numerical simulation tool to investigate the shearing failure mechanism at the interaction surfaces of the rock-rock-bolts during the rock reinforcement process of engineering rock structures. PFC2D is based on the explicit finite difference approach considering the joints and discontinuities in the rock masses known as discrete element method (DEM). In PFC2D, the basic geometry and mechanical properties of the particles in form of contact and parallel bonds, and force and moments are defined for a group of particles gathered as a modelled assembly representing the desired geo-mechanical problem. The micro-mechanical characteristics of the modelled particle assembly are calibrated and assigned properly based on the results of real macro-mechanical properties gained from the standard uniaxial compression and Brazilian tensile strength tests carried out in a rock mechanics laboratory. The parallel bonds are usually used to model the rock joints in the particle assemblies based on those proposed and used by Potyondy and Cundall [42] or Park and Song [36]. The micro-mechanical properties between the particles in an assembly are similar to those obtained for rocks and geo-materials in the literature [43-45]. The inherent properties pertaining to the matrix and cementing between the particles demonstrate the strength of the geomaterial samples [46, 47]. As shown in Figure 1, the parallel interfaces between the contacted particles are considered to provide linear parallel bonds assuming linear elastic and frictional interface behaviors, infinitesimally. These models do not bear any relative sliding and rotation at the beginning. Then, in the interaction surfaces of the assembly, a linear elastic bonded interface of a finite size (not infinitesimal) is assigned which can

transmit the force and bear the moment due to deformation, compression, shear and torsion [41]. The mechanical behavior of parallel bonds obeys the linear elastic behavior up to strength limit of the brittle material. As the applied forces reach beyond the elastic strength limit of the material, the parallel bonds break away and remove from the system as no rotational resistance can be existed at the contact surfaces. The other mechanical characteristics such as intergranular viscous behavior of the particles in the modelled assembly can be achieved through random microstructure and transferring the torque into torsional stress showing the rotational impedance of the particles. It means that the normal and shear force components of the parallel bond force cause linear velocity while the moment components of the parallel bond produce bending moment and rotational movement (twisting) of the particles.

$$F_c = F^1 + F^d + \bar{F} \quad (1)$$

$$M_c = \bar{M} \quad (2)$$

$$\bar{F} = -\bar{F}_n n_c + \bar{F}_s \quad (3)$$

$$\bar{M} = \bar{M}_t n_c + \bar{M}_b \quad (4)$$

Where the linear dashpot and parallel bond forces are denoted as: F^l, F^d and $\bar{F}$, respectively. The parallel-bond moment is denoted as $\bar{M}$. The parallel bonds break away at the stresses beyond the elastic strength i.e., due to overstressing, bending and stretching.

$$\bar{\sigma}_n = \frac{\bar{F}_n}{A} + \bar{\beta}\frac{\bar{M}_b \bar{R}}{\bar{I}} \quad (5)$$

$$\bar{\tau} = \frac{\bar{F}_s}{\bar{A}} + \bar{\beta}\frac{\overline{|M_t|}\,\bar{R}}{\bar{J}} \quad (6)$$

Where the components of normal and shear stresses are denoted by $\bar{F}_n$, $\bar{F}_s$ and the components of bending and twisting moments are indicated by $\bar{M}_b$, $\bar{M}_t$, respectively and the default of moment contribution facto is $\bar{\beta} = 1$. It is evident that when, $\sigma_{max} \geq \bar{\sigma}_n$ or $r_{max} \geq \bar{r}$, the strength of the parallel bonds is exceeded, causing the cemented contact between particles breaks away and resulting in the failure of the assembly. The tensile and shear strengths of the cemented contact of the particles are denoted by $\bar{\sigma}_n$ and $\bar{\tau}$, respectively.

The geometrical characteristics of the cross-sectional surface of the parallel band:

$$\bar{R} = \bar{\lambda} \min (R^{(1)}, R^{(2)}) \quad (7)$$

$$\bar{A} = \pi \bar{R}^2 \quad (8)$$

$$\bar{I} = \frac{1}{4}\pi \bar{R}^4 \quad (9)$$

$$\bar{J} = \frac{1}{2}\pi \bar{R}^4 \quad (10)$$

Where the area of the bond's cross section is $\bar{A}$, the moment and polar moment of inertias of the cross section are $\bar{I}$ and $\bar{J}$, respectively.

The crack propagation mechanism through the parallel bonds can be obtained by the embedded fish language provided in PFC software. Figure 1 illustrates the fracture and failure mechanism of the geomaterial specimens modelled in PFC. The numerical simulation of rock samples focuses on the rock fracturing mechanism due to microcosmic characteristics. The linear elastic behavior is observed at the first stages and the deformation process is continued to the failure and fracturing stage of the modelled sample. The bonds of the model are assumed to break due to the initiation and propagation of normal and shear cracks. As shown in Figure 1, when the normal stress exceeds that of the normal strength of the bond, the tensile cracks are formed in the sample. The shear cracks are produced due to the formation of shear failure when the microcracks cause stress redistribution during the applied compressive loading process of the modelled geomaterial assemblies.

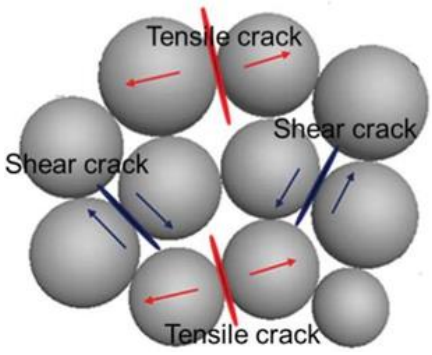

Figure 1. The fracture mechanism between particles; red indicates the tensile crack and blue indicates the shear crack.

2. Numerical simulation of cable bolt based on punch shear test concept using PFC2D

2.1. Micro parameters of the rock Sample

In this study, the modelled particle assemblies have been prepared in PFC2D based on the standard process described by Potyondy and Cundall [42]. The main process includes the

particles' generation and packing, particles' bonding and isotropic stress installations, and elimination of floating (unbonded) particles in the modelled geomaterial assembly. The stress gradients induced due to gravity effect are neglected as the modelled geomaterial specimens are of relatively small sizes so that the macroscopic characteristics can be ignored in their numerical analyses. The micro-properties used for the numerical analyses of the modelled assemblies in PFC2D are calibrated based on the results of Brazilian tensile and uniaxial compressive strengths tests on the real geomaterial specimens carried out in laboratory. In this research, the micro-properties given in Fu et al. [48], are adopted for the standard calibration of parameters used for the PFC2D models. Then, the proper particle assembly is calibrated for the geomaterial (e.g., concrete) sample. The numerical results for the simulated uniaxial compressive test are shown in Figure 2. In this figure, the tensile and shear cracks are denoted by black and red lines, respectively. This is a typical compressive failure pattern similar to that observed in the numerical simulation of the uniaxial compressive strength test (the shear cracks are embedded by the tensile cracks). The mechanical characteristics of the modelled samples are well-matched with experimental test results.

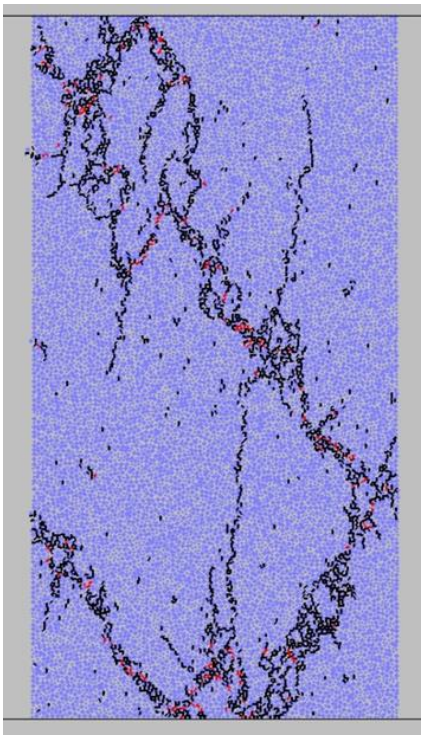

Figure 2 Numerical compression test results

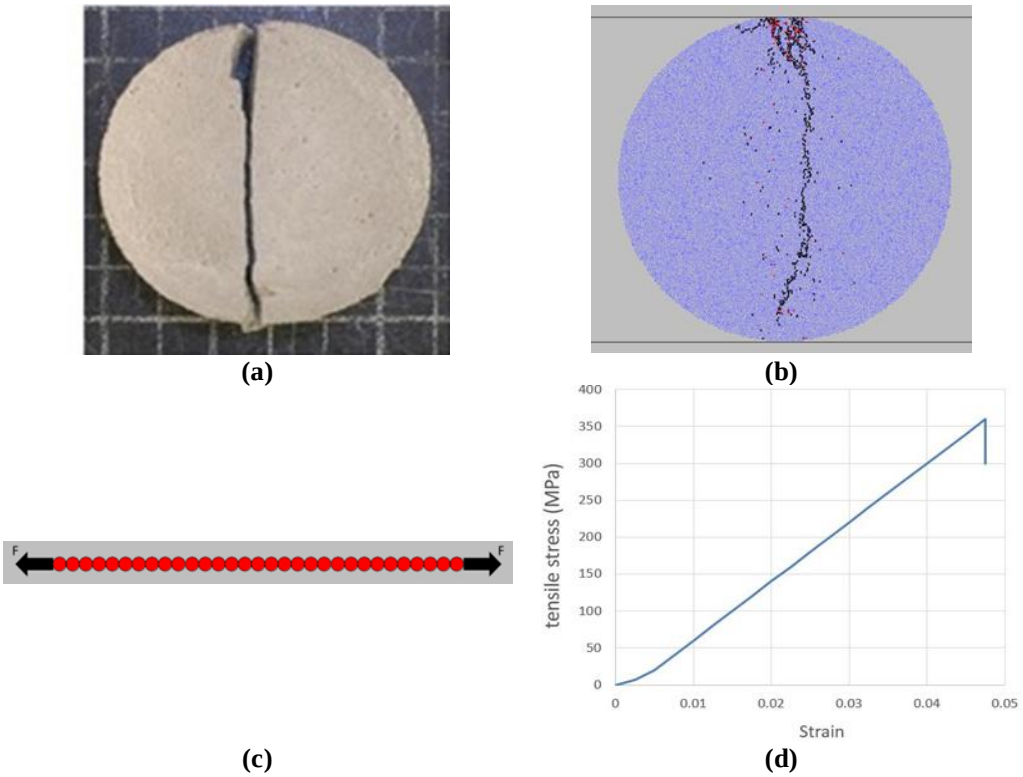

(a) **(b)** **(c)** **(d)**

Figure 3. Failure pattern in a) physical sample, b) PFC2D model, c) bolt under tensile load, d) tensile stress versusstrain for rock bolt.

Although this study focused on the tensile failure behavior of rock bolts, the interface betweenbolt and rock material was necessary to be determined. These properties should be different from the mechanical properties of intact material and rock bolt. In this study, mechanical properties of interfacewere chosen to be less than rock material. Adopting the micro-properties

listed in Fu et al. [49], and the standard calibration procedures [42], a calibrated PFC particle assembly was created for bolt-rock material interface.

In the numerical simulation process, the cable bolt is modelled by a cluster of balls (discs) and their related parallel bonds which transmits the bonding forces and moments between the balls based on the force-displacement (Hook's) law (Figure 3(a) and Figure 3(b)). This condition can model the stress state in a cable bolt. Figure 3(c) demonstrates the microparameters determined from the results obtained for a cable bolt during the pull-out test. The mechanical behavior (stress-strain curve) of the cable bolt's pull-out test is given in Figure 3(d). The adjusted microparameters for the cable bolt are listed in Table 1. The tensile strength of the cable bolt is taken as 360 MPa. Therefore, in the numerical simulation of the pull-out test, when the axial stress in the cable bolt exceeds that of the strength of the parallel bonds, the bonds break away and the bearing capacity of the bolt is lost.

Table 1. Micro parameter of rock bolt.

Micro parameters	value	Micro parameters	value
disc radius (mm)	1	Parallel bond normal strength (MPa)	350±20
Disc density (kg.m^{-3})	3500	Parallel bond shear strength (MPa)	250±20
Disc contact modulus (GPa)	35	Parallel bond stiffness ratio	2.5
Disc stiffness ratio	1.3	Parallel bond radius multiplier	1
Disc friction coefficient	7	Parallel modulus (GPa)	35

2.2. model preparation using Particle Flow Code

After calibration of PFC2D, punch shear test was simulated by creating a rectangular rock model in PFC2D (using the calibrated micro-parameters) (Figure 4-12). The PFC specimen had dimension of100 cm 100 cm. One rock bolt with different indent shape and numbers were inserted within the model. The length, wide and number of rebars were changed to study the influence of rebar shape on the failure mechanism of rock. Rock bolt was created by cluster particle model. Dimension of one indent were (ab in Figures4-6), 15cm20cm (Figure 4a), 15cm30cm (Figure 4b), 15cm40 cm (Figure 4c), 30cm20cm (Figure 5a), 3030cm (Figure 5b), 30cm40cm (Figure 5c), 45cm20cm (Figure 6a), 45cm30 cm (Figure 6b), 45cm40cm (Figure 6c). Dimension of two indents were (ab in Figures7-9), 7.520cm (Figure 7a), 7.5cm30cm (Figure 7b), 7.5cm40cm (Figure 7c), 15cm20 cm (Figure 8a), 15cm30cm (Figure 8b), 1540cm (Figure 8c), 22.5cm20cm (Figure 9a), 22.5cm30cm (Figure 9b), 22.5cm40 cm (Figure 9c), Dimension of three indents were (ab in Figures10-12), 520cm (Figure 10a), 5cm30cm (Figure 10b), 5cm40cm (Figure 10c), 10cm20 cm (Figure 11a), 10cm30cm (Figure 11b), 1040cm (Figure 11c), 15cm20cm (Figure 12a), 15cm30cm (Figure 12b), 15cm40 cm (Figure 12c). When two rebars were situated on the bolt surface, the distance between rebars were 4cm, 6cm and 8 cm. When three rebars were situated on the bolt surface, the distance between rebars were 1cm, 2cm and 3 cm.

The punch shear test is simulated in PFC2D by removing two vertical particle bands from the top and bottom of the particle assembly model as shown in Figures 4 to 7. Then, shear forces are applied to the upper and lower walls and confining pressure is applied to the right and left walls of the assembly, respectively. The shear force is applied to the cable bolt by inserting a normal force to the bolt as the lower wall of the model applies the normal force in the upward direction so that a shear force is produced at the interface of the model and bolt as shown in Figure 4a. The confining pressure is fixed at about one-tenth of the uniaxial compressive strength of the specimen (3.7 MPa in this research). Loading rate of axial force was 0.015 mm/sec. The reaction forces registered on the upper wall during the testing process show the shear force applied to the specimen and the shear stress can be obtained by dividing the shear force to 100 cm and unit thickness (for two-dimensional problems). The running time for each simulation conducted in the study was 50 minutes.

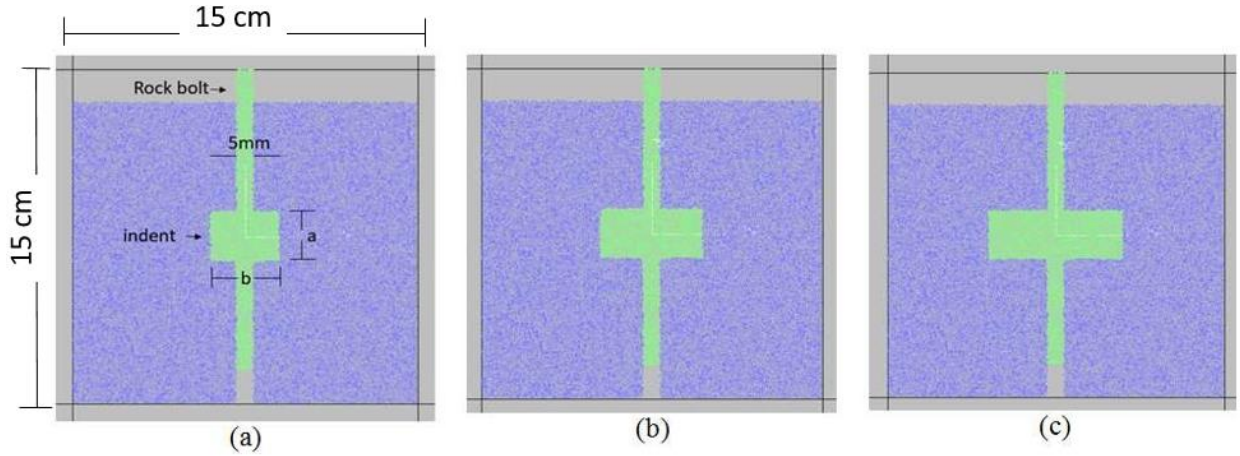

Figure 4. One indent with dimension of (ab); a) 15mm20mm, b) 15mm30mm, c) 15mm40 mm.

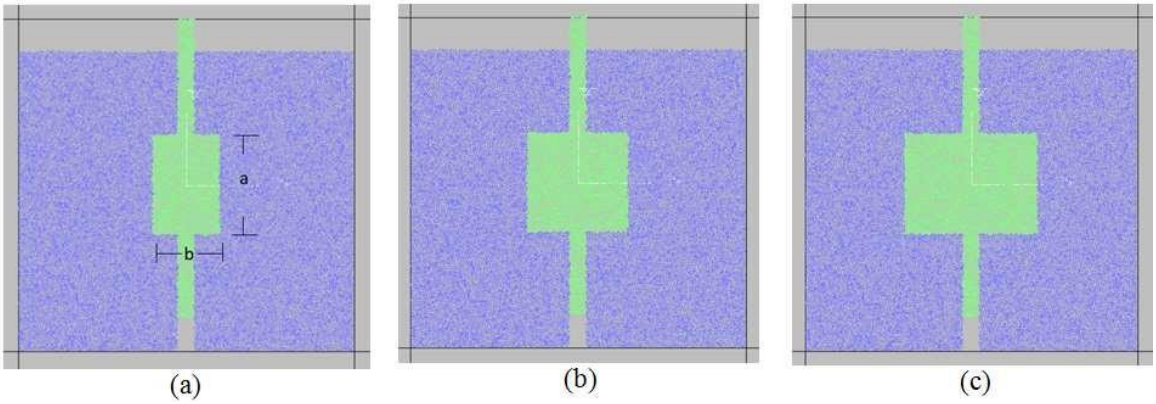

Figure 5. One indent with dimensions of (ab); a) 30cm20cm, b) 30cm30cm, c) 30cm40 cm.

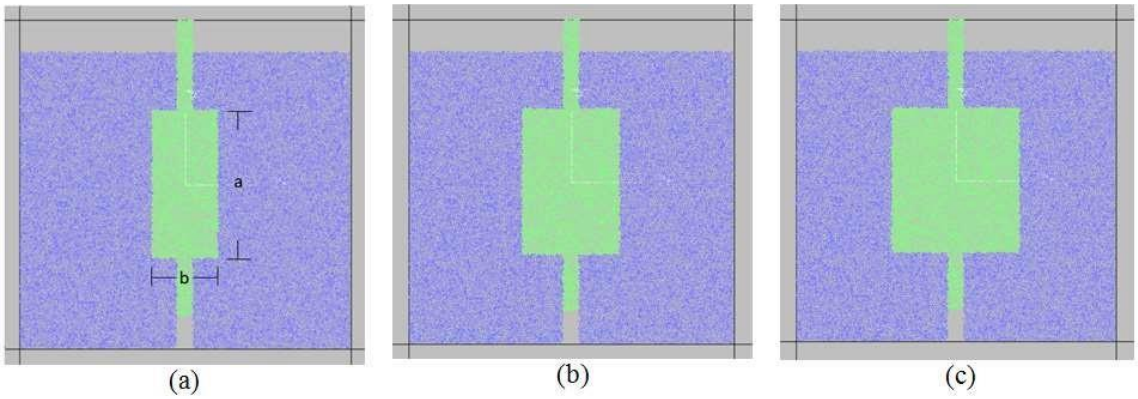

Figure 6. One indent with dimensions of (ab); a) 45cm20cm, b) 45cm30cm, c) 45cm40 cm.

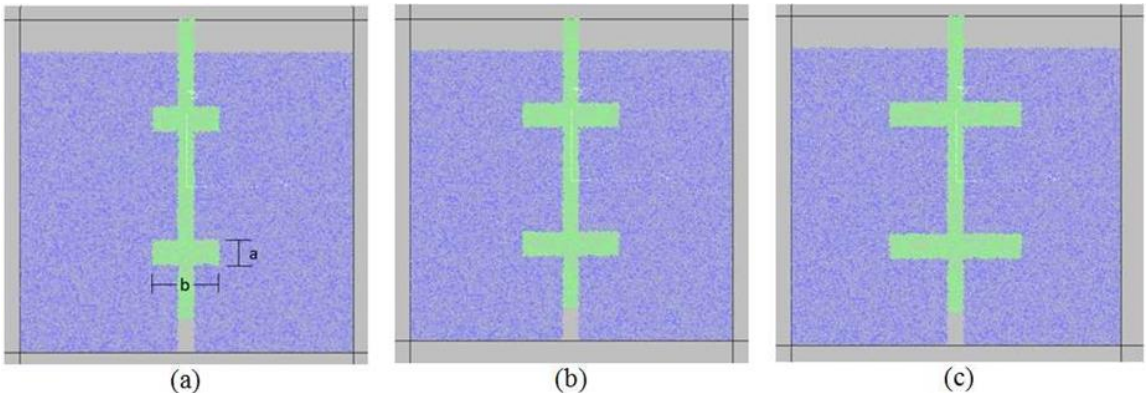

Figure 7. Two indents with dimensions of (ab); a) 7.5cm20cm, b) 7.5cm30cm, c) 7.5cm40 cm.

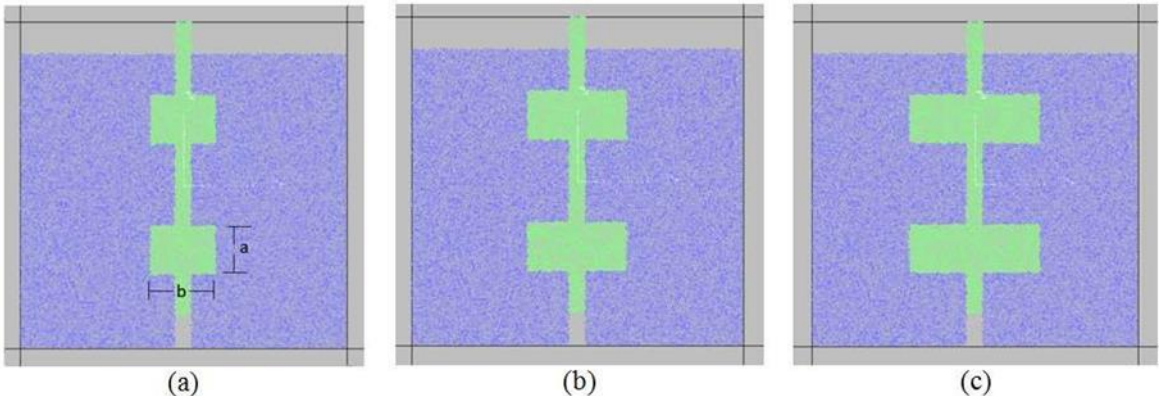

Figure 8. Two indents with dimensions of (ab); a) 15cm20cm, b) 15cm30cm c), 15cm40 cm.

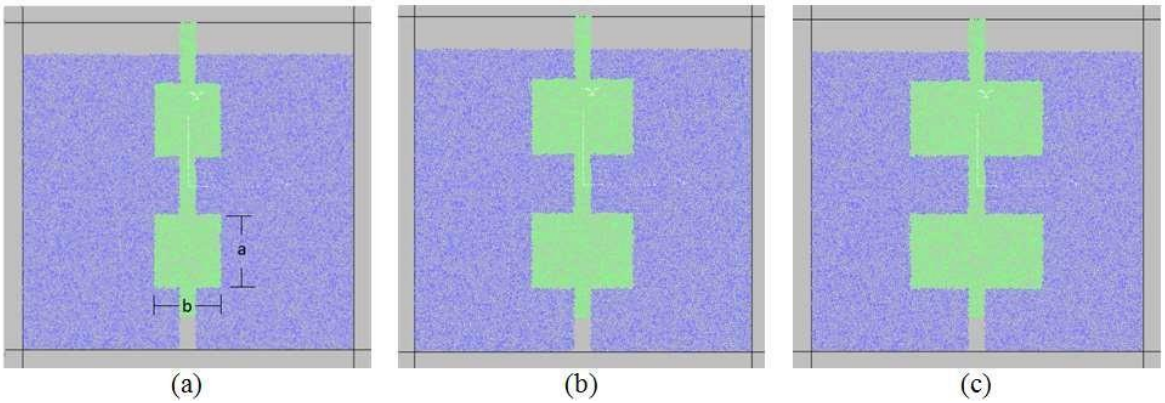

Figure 9. Two indents with dimensions of (ab); a) 22.5cm20cm, b) 22.5cm30cm, c) 22.5cm40 cm.

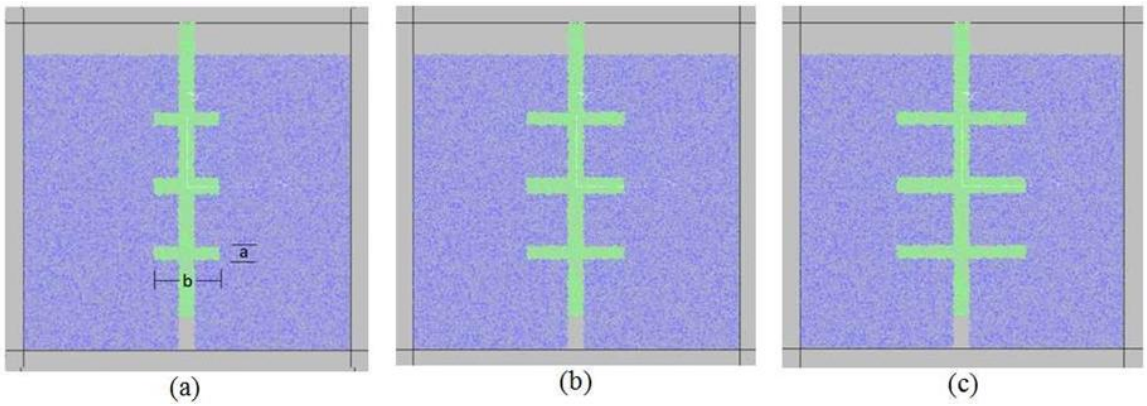

Figure 10. Three indents with dimensions of (ab); a) 5cm20cm, b) 5cm30cm, c) 5cm40 cm.

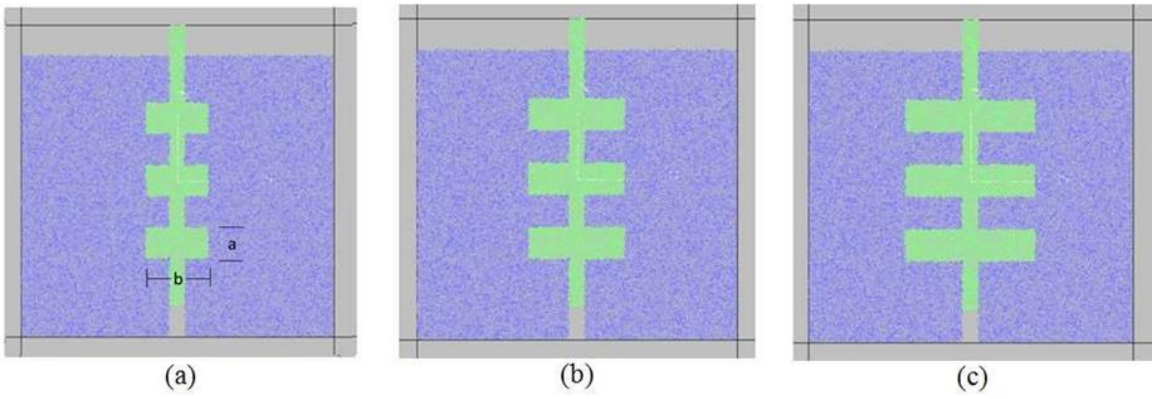

Figure 11. Three indents with dimensions of (ab); a) 10 cm20cm, b) 10 cm30cm, c) 10 cm40 cm.

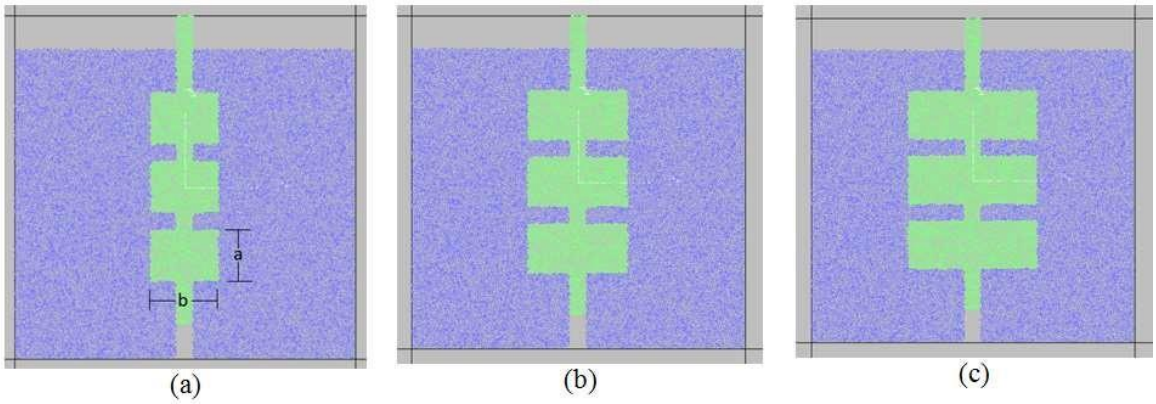

Figure 12. Three indents with dimensions of (ab); a) 15cm20cm, b) 15cm30cm, c) 15cm40 cm.

3. Numerical modeling outputs:

3.1. The impact of a single indent on the breakage pattern in the numerical model.

The failure patterns of the models are displayed in Figure 15-13 to analyze the effect of the bolt indent dimension. In these models, the display of tensile cracks and shear cracks is specified by a black line and a red line respectively.

a) bolt length was 15 cm (a in Figure 4a):

For the bolt length of 15 cm, Figure 13(a) demonstrates the failure process of the modelled specimens having indents of 20 cm in width. The tensile (primary) cracks initiate at the interface of the cable bolt and rock at the beginning and then propagate in the model during the failure stage. It has been shown that four tensile cracks are induced from the indent tip and extend toward the surface of the cable bolt-rock interface. Figure 13(b) shows the initiation of tensile crack at the interface of the cable bolt and rock for the specimens of 30 cm in indent width. These cracks extend to the edge of modelled specimen during the loading process. Again, four tensile cracks are induced and propagate from the indent tip and meet the interface of the bolt-rock specimen. Figure 13(c) demonstrates the case of modelled specimens with 40 cm indent widths. In this case, the tensile and wing cracks are initiated at the interface and from the tip of the indent, but two rock wedges are produced. Therefore, it is concluded that the rock wedge dimensions increase as the indent width increases.

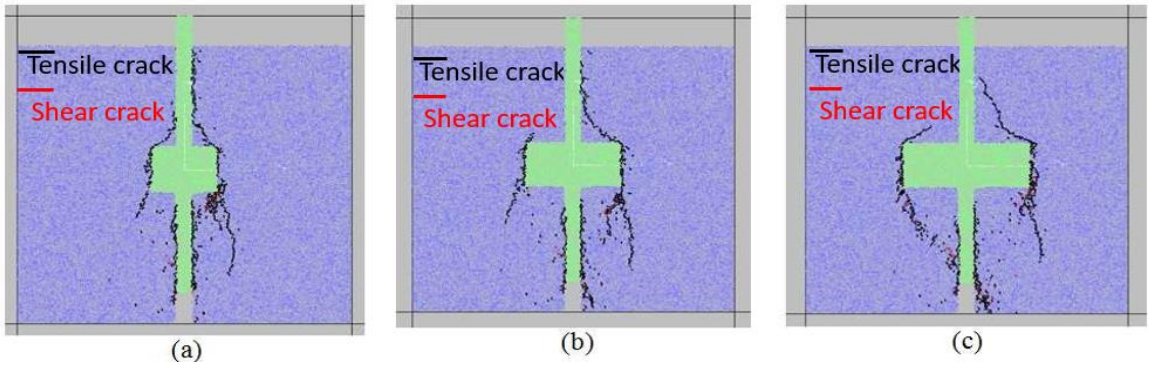

Figure 13. Failure pattern in models consisting one indent with dimensions of (ab); a) 15cm20cm, b) 15cm30cm, c) 15cm40 cm.

b) bolt length was 30 cm (a in Figure 5a):

For the bolt length of 30 cm length and when the width of the cable bolt indent is 20 cm, the tensile cracks are produced at the interaction surface between the rock and the cable bolt (in the beginning of failure process) and propagate towards the boundaries of the specimen at final failure stage (Figure 14(a)). Four wing cracks are also created at the indent tip and propagate towards the intersection surface and boundaries of the modelled specimen. The same phenomena are repeated for the cases of 30 cm and 40 cm cable bolt widths as shown in Figure 14(b) and 14(c), respectively. These results show that as the width of the cable bolt indents increases, the dimensions of the rock wedges (formed from the coalescences of the induced tensile cracks) increase accordingly.

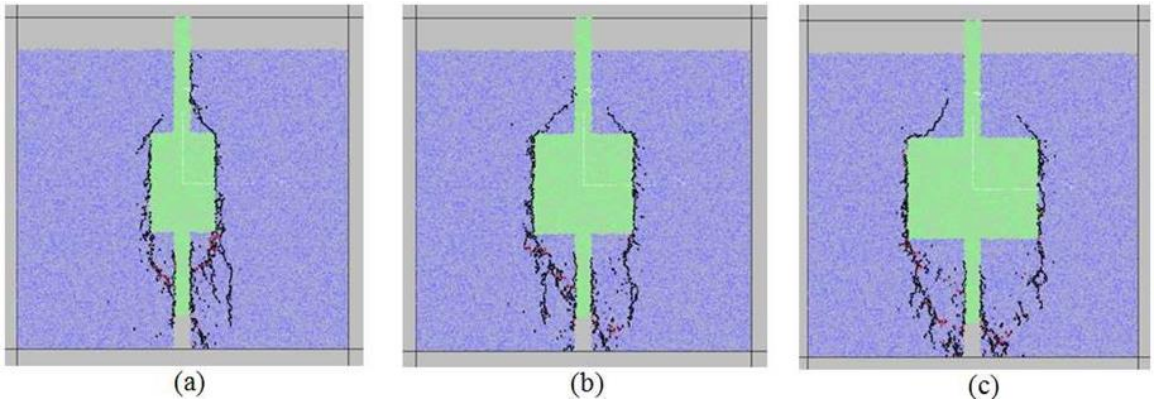

Figure 14. Failure pattern in models consisting one indent with dimensions of (ab); a) 30cm20cm, b) 30cm30cm, c) 30cm40 cm.

c) bolt length was 45 cm (a in Figure 6a):

For a bolt length of 45 cm and when cable bolt indent width is 20cm (Figure 15a), the tensile wing cracks are induced between the cable bolt and rock interface at the beginning of failure process, and then continue their propagation to the model boundaries. On the other hand, four induced wing cracks also start their propagation from the indent tip and extends towards the interface and boundaries of the modelled specimen. When the indent widths increase to 30 cm (Figure 15 (b)) and 40 cm (Figure 15(c)), again the tensile cracks are induced at the interfaces of the cable bolt and rock in the modelled specimens. The induced wing cracks also start their initiation and propagation from the indent tips and extend towards the interfaces and boundaries of the modelled samples. However, the dimensions of the rock wedges increase as the indent width of the cable bolt increases (because of the coalescences of the wing cracks).

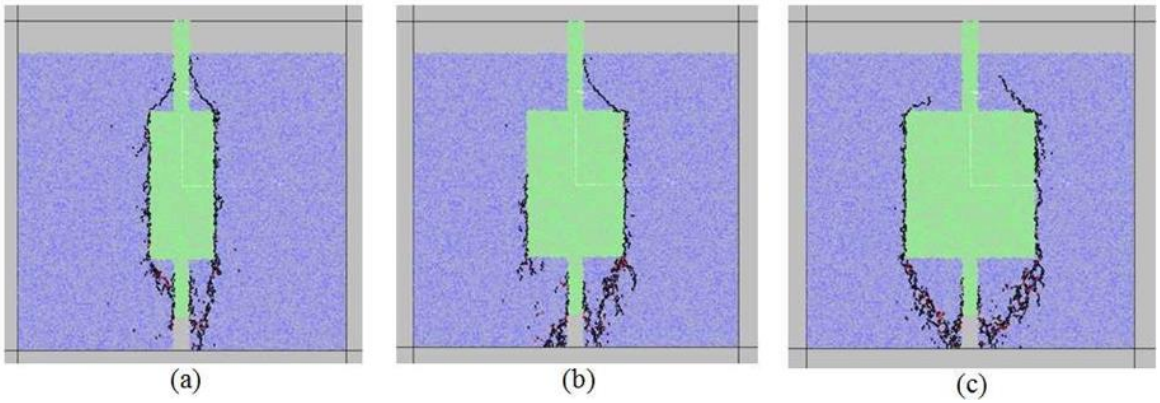

Figure 15. Failure pattern in models consisting one indent with dimensions of (ab); a) 45cm20cm b), 45cm30cm c), 45cm40 cm.

3.2. The effect of two indent on the failure pattern of numerical model

The influence of the bolt indentation size on the breakage behavior of the numerical model depicted in Figures 16-18. In these models, the display of tensile cracks and shear cracks is specified by a black line and a red line, respectively.

a) bolt length was 7.5 cm (a in Figure 7a):

When the length of cable bolt reduces to that of 7.5 cm as shown in Figure 7(a), changing the width of the indent from 20 cm to 45 cm, the mechanism of failure pattern and crack propagation within the modelled sample is as follows:

When the indent width of the cable bolt is fixed at 20 cm (Figure 16(a)), the primary tensile cracks are induced in the modelled specimen and eight cracks may initiate from the indent tip and propagate to meet the cable bolt-rock interface. when the indent width is fixed at 30 cm as shown in Figure 16(b), the tensile cracks are induced at the interface of the rock and cable bolt. In this case, again eight wing cracks are induced at the indent tip and extend diagonally within the modelled

sample till meet the specimen's boundaries. As the indent width of the cable bolt reaches to 45 cm (Figure 16(c)), the tensile cracks are also induced in the model and at the tip of the indent but two rock wedges are formed at the failure stage and the dimensions of the wedges increases as the indent width increases.

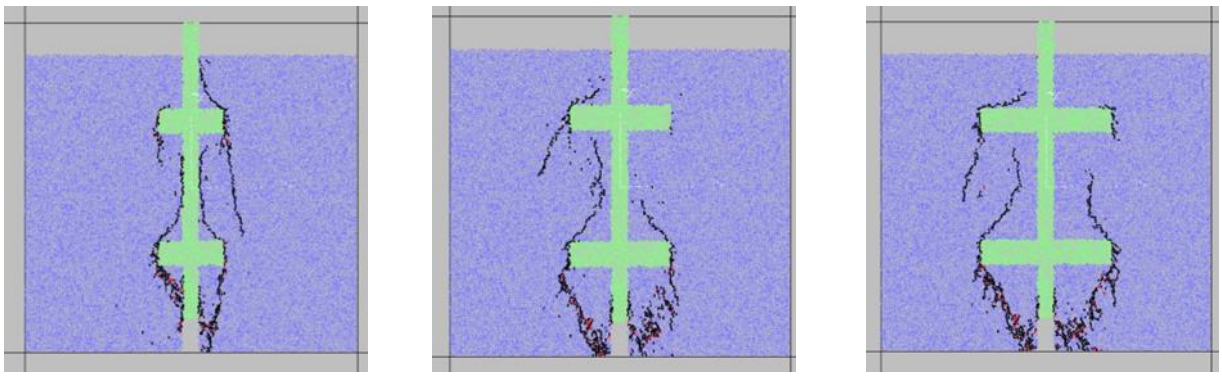

(a) (b) (c)

Figure 16. Failure pattern in models consisting two indents with dimensions of (ab); a) 7.5cm20cm b), 7.5cm30cm c), 7.5cm40 cm.

b) bolt length was 15 cm (a in Figure 8a):

when the cable bolt length increases to that of 15 cm, and when the width of the indent reaches to that of 20 cm as shown in Figure 17(a), the tensile cracks are induced at the interface of the rock and cable bolt, and also eight wing cracks may be initiated from the indent tip and propagate within the model till meet the boundary of the geomaterial sample. Figure 17(b) shows the crack propagation paths and the coalescences of the induced tensile cracks at the cable bolt-rock interface and the indent tips when the indent width is 30 cm. Figure 17(c) demonstrates the failure and fracturing process in the modelled samples with the indent width of 40 cm. In this case two wedges of the failed rock are formed and their dimensions increase with the increase in indent width of the modelled specimens.

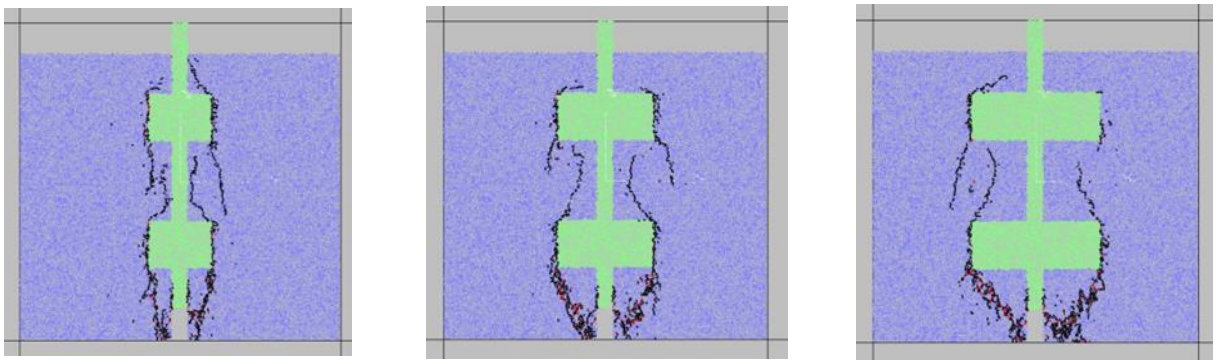

(a) (b) (c)

Figure 17. Failure pattern in models consisting two indents with dimensions of (ab); a) 15cm20cm b), 15cm30cm c), 15cm40 cm.

c) bolt length was 22.5 cm (a in Figure 9a):

The modelled specimen for a cable bolt of length 22.5 cm with a cable bolt indent width 20 cm is shown in Figure 18(a). The tensile cracks are initiated from the interface of the cable bolt-rock and from the tip of the indent during the failure process. These cracks propagate within the model and extend toward the specimen's boundaries and interface surface. Figure 18(b) and Figure 18(c) demonstrate the fracturing process of the modelled samples with 30 cm and 45 cm indent widths, respectively. In these models, the wing cracks are induced at the interface of rock and cable bolt. Eight cracks are initiated from the indent tips of the specimens. These induced wing cracks propagated within the specimens and may extend toward the boundaries and interfaces of each sample or they may coalesce with one another to make the rock wedges (two wedges are produced in each model). It has been concluded that as the indent width increases the dimensions of the rock wedges increase.

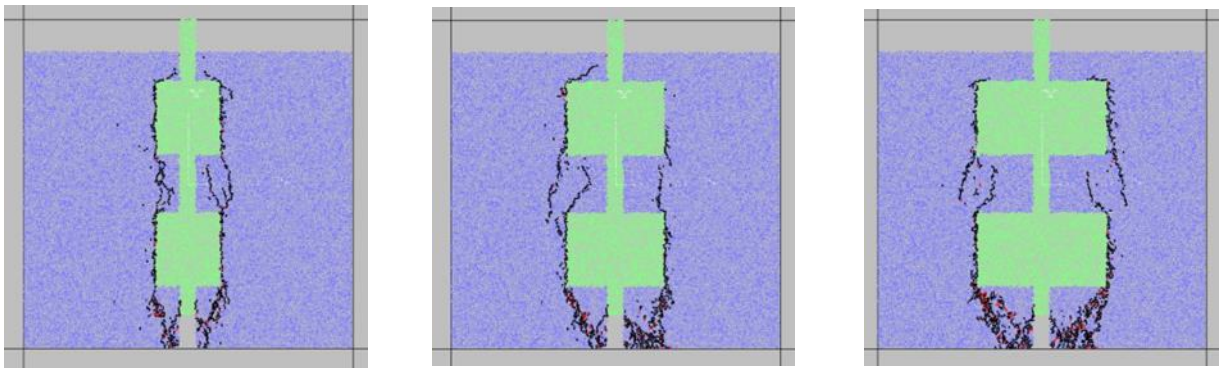

(a) (b) (c)

Figure 18. Failure pattern in models consisting two indents with dimensions of (ab); a) 22.5cm20cm b), 22.5cm30cm c), 22.5cm40 cm.

3.3. The effect of three indent on the failure pattern of numerical model

The influence of the bolt indentation size on the breakage behavior of the numerical model is depicted in Figures 19-21. In these models, the display of tensile cracks and shear cracks is specified by a black line and a red line, respectively.

a) bolt length was 5 cm (a in Figure 10a):

Figure 19(a) illustrates the fracturing and failure process of a modelled sample containing a cable bolt of 5 cm with indent thickness of 20 cm. The tensile cracks are induced at the interaction surface of the cable bolt and rock at the beginning. Then, eight induced tensile cracks are initiated from the indent tip and extend toward the specimen's boundary or coalesce with one another and form rock wedges. Then the cable bolt-rock indent width is increased to 30 cm and the failure process of the modelled specimen is analyzed as shown in Figure 19(b). In this case again the tensile cracks are induced in the cable bolt-rock interface and eight of them are initiated at the indent tip of the model. Finally, Figure 19(c) demonstrates the fracturing pattern of the modelled cable bolt-rock specimen with indent thickness of 40 cm. Again, the tensile cracks are initiated at the interface and at the indent tip. They propagate and meet one another or extend toward the boundaries of the sample. Therefore, it is visualized that as the indent width of the cable bolt-rock models increases, the sizes of the rock wedges increase accordingly.

The indentation caused eight wing cracks to start from the tip and spread diagonally until they met a bolt-rock interface. As a result, two rock wedges were formed. The wedge dimension increases with the increase of the indent width.

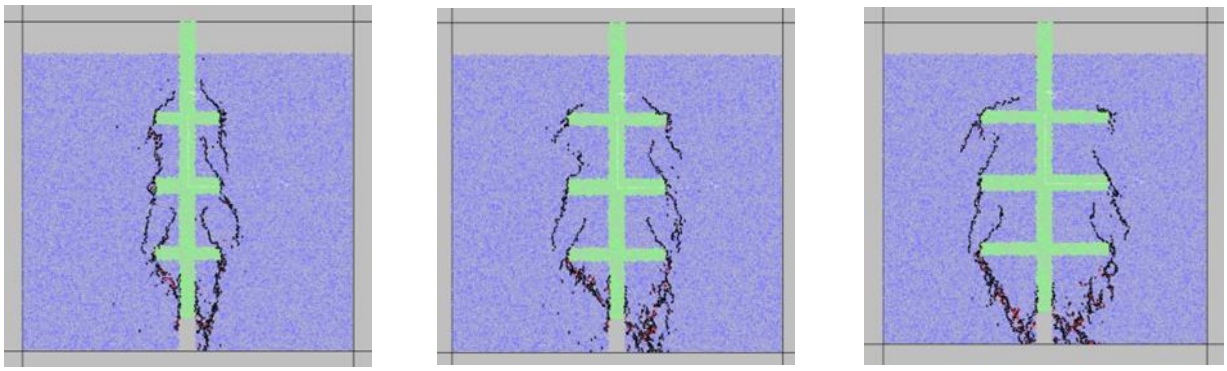

(a) (b) (c)

Figure 19. Failure pattern in models consisting three indents with dimensions of (ab); a) 5cm20cm b), 5cm30cmc), 5cm40 cm.

b) bolt length was 10 cm (a in Figure 11a):

Considering different bolt indent widths of 20 cm (Figure 20(a)), 30 cm (Figure 20(b)) and 40 cm (Figure 20(c)) for a bolt of 10 cm length in the modelled specimens, the crack propagation patterns and the failure mechanisms of the cable bolt-rock interface are investigated. The results show that in all models, the tensile cracks are induced at the interfaces and eight cracks are initiated from the indents tips and propagated

within the models till coalesce with one another or meet the boundaries of the model. It has also been concluded that as the indent width and length of the cable bolt increase, the sizes of the rock wedges increase for all modelled specimens.

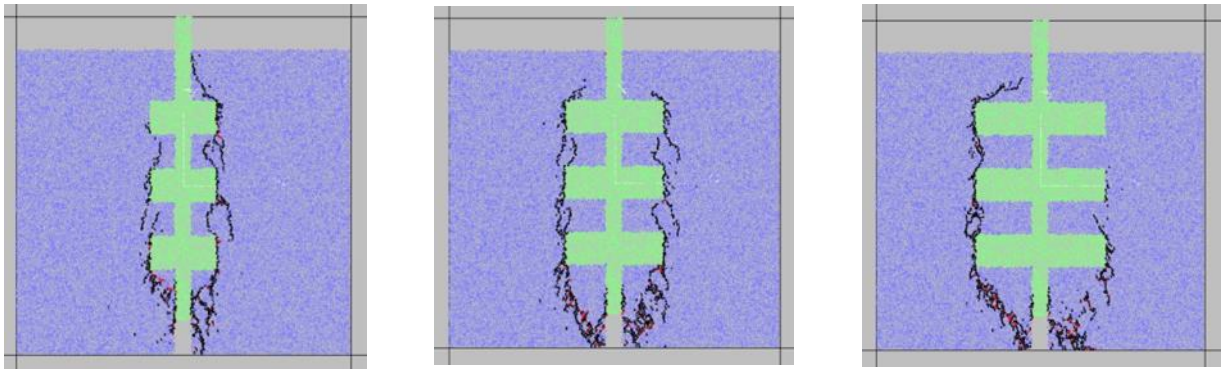

(a) (b) (c)

Figure 20. Failure pattern in models consisting three indents with dimensions of (ab); a) 10 cm20cm b), 10 cm30cm c), 10 cm40 cm.

c) bolt length was 15 cm (a in Figure 12a):

The same models are repeated for the cable bolt length of 15 cm. Figure 21(a) shows the model considering the indent width of 20 cm, Figure 21(b) demonstrates the model for 30 cm indent width and Figure 21(c) illustrates the model for the case of 40 cm indent width. The crack propagation paths and the failure and fracturing mechanism of these models are the same as the previous models and demonstrate the effects of indent widths on the failure mechanism of cable bolt-rock interactions. Tensile cracks were initiated in the first of the axial loading but shear cracks were initiated when rock bolt reach the final loading capacity. Shear cracks were initiated from frictional behavior and sliding displacement between broken fragments.

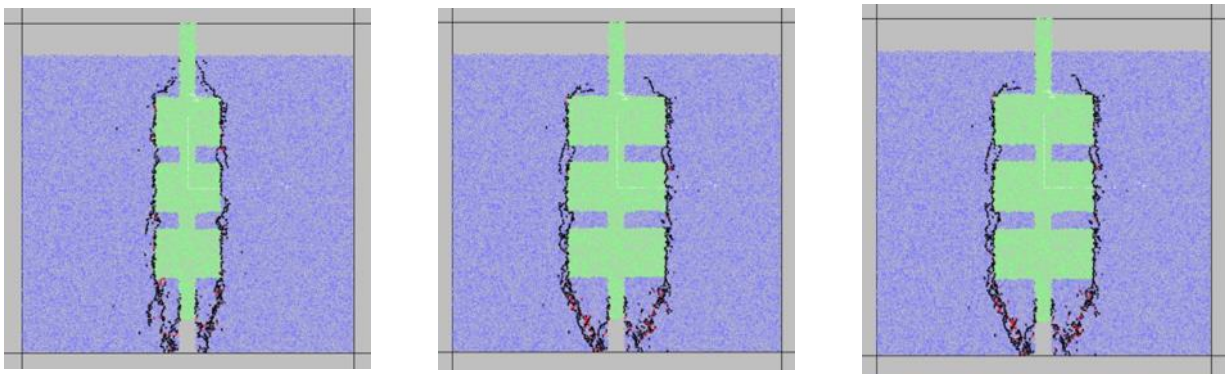

(a) (b) (c)

Figure 21. Failure pattern in models consisting three indents with dimensions of (ab); a) 15cm20cm b), 15cm30cm c), 15cm40 cm.

3.4. The effect of rock bolt indent dimension and indent number on the shear strength of numerical model

Figure 22(a-c) shows the effect of rock bolt indent dimension on the shear strength of numerical model. The results show that as the cable bolt indent width increases, the shear strength of the model at the interaction surface of the bolt-rock increases.

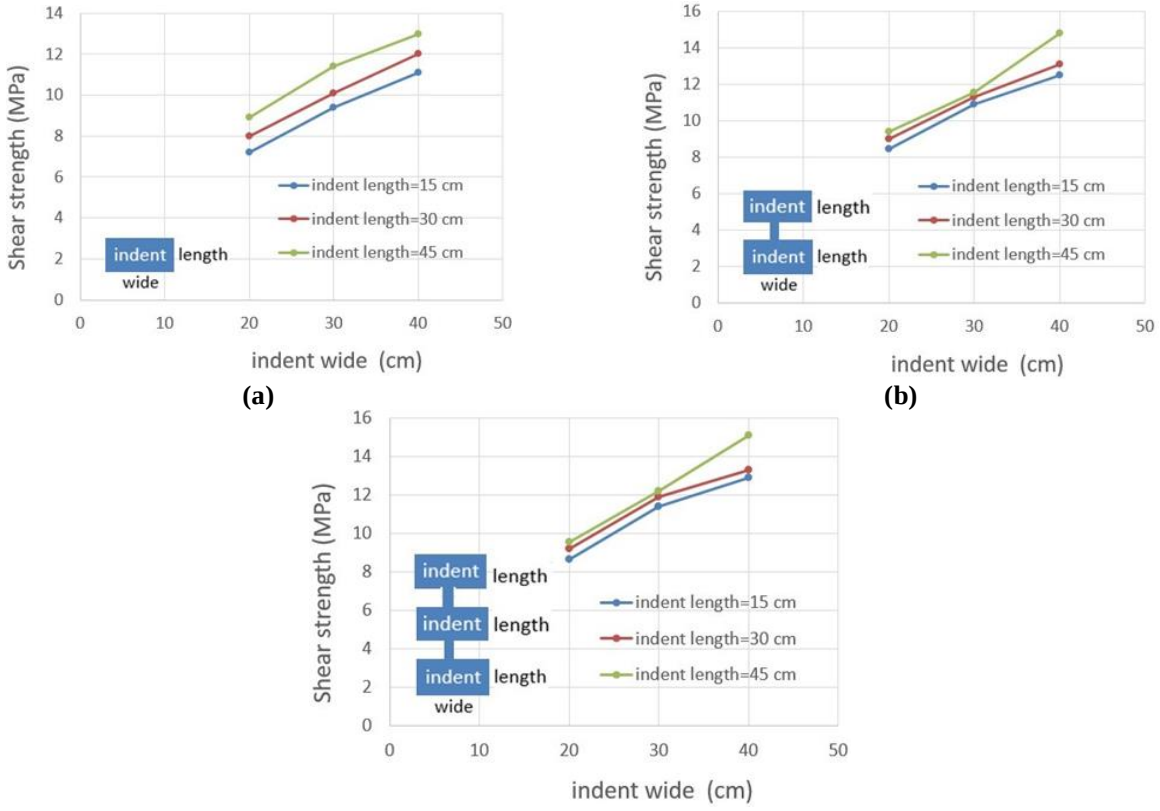

Figure 22 The effect of rock bolt indent width on the shear strength of numerical model, a) one indent, b) twoindents, c) three indents.

The shear behavior of the numerical model, as shown in Figure 23(a-c), indicates that the shear strength increased with the number of rock bolt indents.

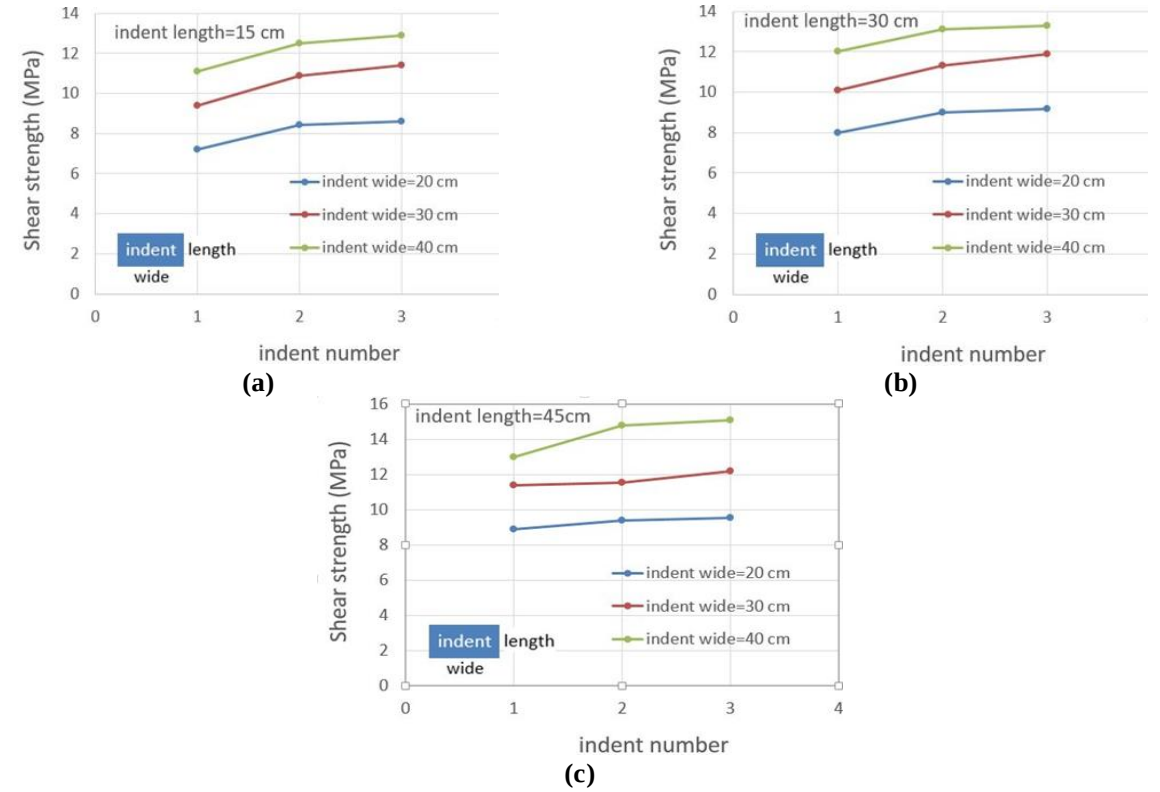

Figure 23 The effect of rock bolt indent number on the shear strength of numerical model; indent length was, a)15cm, b) 30cm, c) 45cm.

3.5. Verification of failure pattern of rock bolts

Figure 24 shows experimental failure pattern of rebar bolts [50]. The base model, which was concrete and grout, has been used as filling material between rebar bolts and concrete. The mechanical properties of grout were less than the concrete mechanical properties. The results show that the tensile cracks occur in grout and also a wedge failure occurs in attachment surface of grout with bolt. This failure was similar to numerical testing results obtained in this research (Figures13-21).

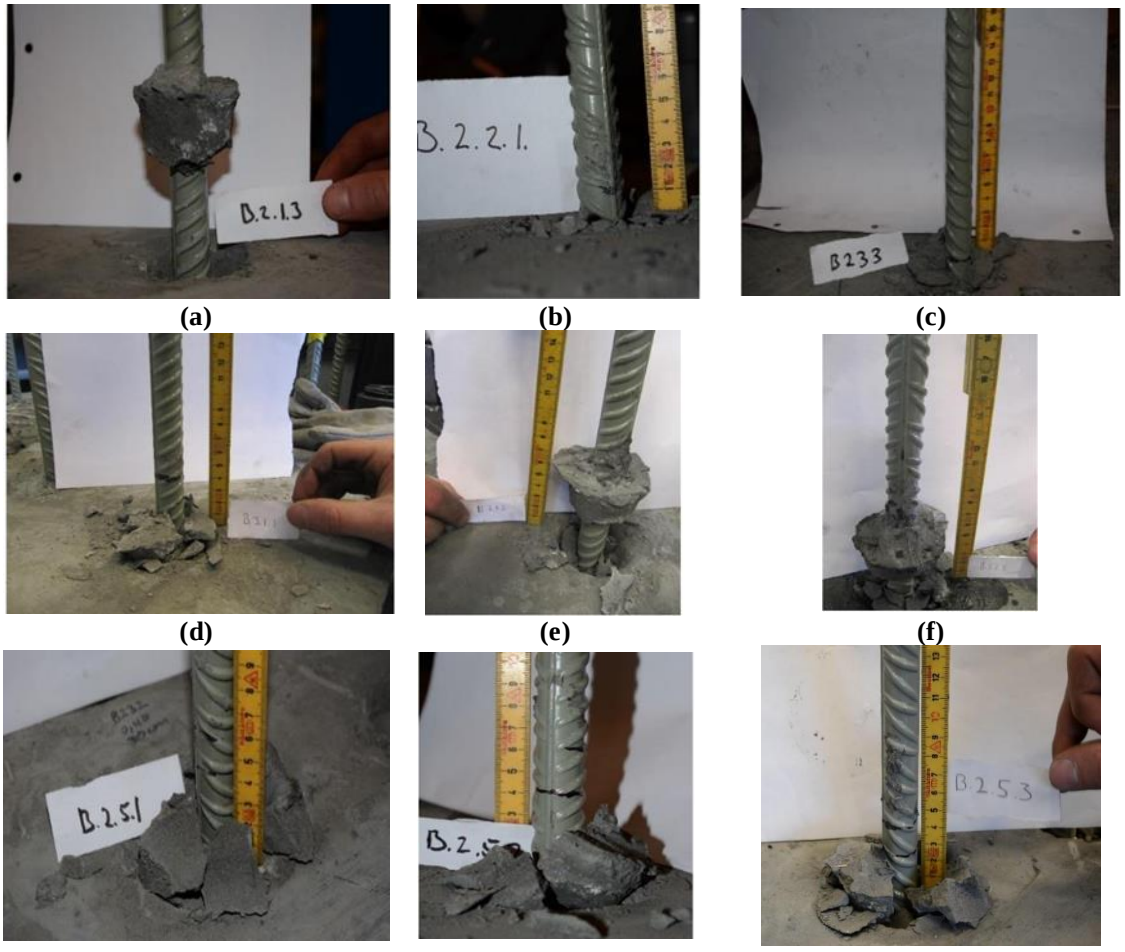

(a) (b) (c)

(d) (e) (f)

(g) (h) (i)

Figure 24. Failure pattern of rock bolts under tensile loading [50].

4. Conclusions

The effects of cable bolt indent size on the mechanical behavior and shear strength of the bolt-rock interface are numerically investigated by discrete element modeling analyses using PFC2D. The microparameters for the PFC models are calibrated through standardized uniaxial compressive and Brazilian tensile strengths tests. The particle assemblies of the numerical models are of the dimensions 100 cm 100 cm, prepared and calibrated carefully to precisely model various cable bolt-rock interaction surfaces. The models are provided using the concept of punch through shear tests. The normal load on the modelled sample is fixed as one-tenths of that of the uniaxial compressive strength of the geomaterial specimen ($\sigma_c/10 = 3.7\ MPa$). The following main conclusions are drawn based on the numerical simulation of the problem:

- The tensile cracks are initiated at the interface of the cable bolt and rock when the cable bolt width is 20 cm. Four wing cracks are also induced at the indent tip. The same results are obtained when the cable bolt width reaches to those of 30 cm and 40 cm.
- As the cable bolt width increases, the size of rock wedges increases accordingly due to crack propagation and coalescence.
- When the widths of cable bolt indents increase, the number of induced tensile cracks within the model increase.

- It has been observed that as the cable bolt length increases, the shear strength of the bolt-rock interaction increases.
- Increase in the indent width and indent number of the cable bolt will increase the total shear strength of the model.

References

[1]. Bahrani, N., & Hadjigeorgiou, J. (2017). Explicit reinforcement models for fully-grouted rebar rock bolts. *Journal of Rock Mechanics and Geotechnical Engineering, 9(2),* 267-280.

[2]. Ortlepp, W. D. (1994). Rockburst mechanisms in tunnels and shafts. *Tunnelling and Underground Space Technology, 9(1),* 59-65.

[3]. Kaiser, P. K., Tannant, D. D., & McCreath, D. R. (1996). Canadian Rockburst Support Hand-Book. Geomechanics Research Centre, *Laurentian University*, Sudbury, Ontario, Canada.

[4]. Ortlepp, W. D., & Stacey, T. R. (1998). Performance of tunnel support under large deformation static and dynamic loading. *Tunnelling and Underground Space Technology, 13(1),* 15-21.

[5]. Orelepp, W. D., Bornman, J. J., & Erasmus, N. (2001). The durabara yieldable support tendon-design rationale and laboratory results in Rock bursts and Seismicity in Mines. *South African Inst of Mining and Metallurgy*, Johannesburg, South Africa, 263-266.

[6]. Doucet, A. (2005). Laboratory testing of a new type of energy absorbing rock bolt. *Tunnelling and Underground Space Technology, 20(4),* 291-300.

[7]. St-Pierre, L., Hassani, F. P., & Radziszewski, P. H. (2009). Development of a dynamic model for a cone bolt. *International Journal of Rock Mechanics and Mining Sciences, 46(1),* 107-114.

[8]. Li, C. C. (2010). A new energy-absorbing bolt for rock support in high stress rock masses. International Journal of Rock Mechanics and Mining Sciences, 47(3), 396-404.

[9]. Li, C. C. (2011a). Performance of D-bolts under static loading. *Rock Mechanics and Rock Engineering, 45(2),* 183-192.

[10]. Li, C. C., & Doucet, C. (2011b). Performance of D-bolts under dynamic loading. *Rock Mechanics and Rock Engineering, 45(2),* 193-204.

[11]. Cai, M. (2012). Influence of bolt-grout bonding on MCB cone bolt performance. *International Journal of Rock Mechanics and Mining Sciences, 49,* 165-175.

[12]. Zhang, C. (2012). Case histories of four extremely intense rock bursts in deep tunnels. *Rock Mechanics and Rock Engineering, 45(3),* 275-288.

[13]. He, M., & Gong, W. (2014). Development of a novel energy-absorbing bolt with extraordinarily large elongation and constant resistance. *International Journal of Rock Mechanics and Mining Sciences, 67,* 29-42.

[14]. Zhou, H., & Meng, F. (2014). Analysis of rockburst mechanisms induced by structural planes in deep tunnels. *Bulletin of Engineering Geology and the Environment, 74(4),* 1435-1451.

[15]. Meng, F., & Wong, L. N. Y. (2019). Shear rate effects on the post-peak shear behaviour and acoustic emission characteristics of artificially split granite joints. *Rock Mechanics and Rock Engineering, 33,* 1-20.

[16]. Rezaei, M. (2020). Feasibility of novel techniques to predict the elastic modulus of rocks based on the laboratory data. *International Journal of Geotechnical Engineering, 14(1),* 25-34.

[17]. Asadizadeh, M., & Rezaei, M. (2021). Surveying the mechanical response of non-persistent jointed slabs subjected to compressive axial loading utilizing GEP approach. *International Journal of Geotechnical Engineering, 15(10),* 1312-1324.

[18]. Zhao, T., & Zhang, Y. (2018). Analysis on the creep response of bolted rock using bolted burgers model. *Geomechanics and Engineering, An International Journal, 14(2),* 98-111.

[19]. Kim, H. (2018). Anchorage mechanism and pullout resistance of rock bolt in water-bearing rocks. *Geomechanics and Engineering, An International Journal, 15(3),* 78-91.

[20]. Wang, H., & Li, S. (2019). Investigating the supporting effect of rock bolts in varying anchoring methods in a tunnel. *Geomechanics and Engineering, An International Journal, 19(6),* 81-100.

[21]. Zou, J., & Xia, Z. (2016). Theoretical solutions for displacement and stress of a circular opening reinforced by grouted rock bolt. *Geomechanics and Engineering, An International Journal, 11(3),* 99-111.

[22]. Doucet, A. (2005). Laboratory testing of a new type of energy absorbing rock bolt. *Tunnelling and Underground Space Technology, 20(4),* 291-300.

[23]. He, M., & Gong, W. (2014). Development of a novel energy-absorbing bolt with extraordinarily large elongation and constant resistance. *International Journal of Rock Mechanics and Mining Sciences, 67,* 29-42.

[24]. Li, C., & Stillborg, B. (1999). Analytical models for rock bolts. *International Journal of Rock Mechanics and Mining Sciences, 36(8),* 1013-1029.

[25]. Cai, Y. (2004a). An analytical model to predict axial load in grouted rock bolt for soft rock tunneling. *Tunnelling and Underground Space Technology, 19(6),* 607-618.

[26]. Cai, Y., Esaki, T., & Jiang, Y. (2004b). A rock bolt and rock mass interaction model. *International Journal of Rock Mechanics and Mining Sciences, 41(7),* 1055-

1067.

[27]. Spang, K., & Egger, P. (1990). Action of fully-grouted bolts in jointed rock and factors of influence. *Rock Mechanics and Rock Engineering, 23(3),* 201-229.

[28]. Zhang, B., Li, S., & Xia, K. (2016). Reinforcement of rock mass with cross-flaws using rock bolt. *Tunnelling and Underground Space Technology, 51*, 346-353.

[29]. Ferrero, A. M. (1995). The shear strength of reinforced rock joints. *International Journal of Rock Mechanics and Mining Sciences & Geomechanics Abstracts, 32(6),* 595-605.

[30]. Chen, Y., & Li, C. C. (2015). Experimental and three-dimensional numerical studies of the anchorage performance of rock bolts. Proceedings of the 13th International Congress of Rock Mechanics, Montreal, Canada.

[31]. Golewski, G. L. (2023a). Concrete composites based on quaternary blended cements with a reduced width of initial microcracks. *Applied Sciences, 13(12),* 7338.

[32]. Golewski, G. L. (2023b). Effect of coarse aggregate grading on mechanical parameters and fracture toughness of limestone concrete. *Infrastructures, 8(8),* 117. https://doi.org/10.3390/infrastructures8080117

[34]. Golewski, G. L. (2023d). Study of strength and microstructure of a new sustainable concrete incorporating pozzolanic materials. *Structural Engineering and Mechanics, 86(4),* 431-441.

[35]. Selvadurai, A. P. S., & Yu, Q. (2005). Mechanics of a discontinuity in a geomaterial. *Computational Geotechnics, 32*, 92-106.

[36]. Park, J. W., & Song, J. J. (2009). Numerical simulation of a direct shear test on a rock joint using a bonded-particle model. *International Journal of Rock Mechanics and Mining Sciences, 46*, 1315-1328.

[37]. Dugdale, D. S. (1960). Yielding of steel sheets containing slits. *Journal of the Mechanics and Physics of Solids, 8*, 100-104.

[38]. Qiao, P., & Chen, Y. (2008). Cohesive fracture simulation and failure modes of FRP-concrete bonded interfaces. *Theoretical and Applied Fracture Mechanics, 49*, 213-225.

[39]. Hawileh, R. A., Naser, M. Z., & Abdalla, J. A. (2013). Finite element simulation of reinforced concrete beams externally strengthened with short-length CFRP plates. *Composites Part B: Engineering, 45*, 1722-1730.

[40]. Su, X. T., Yang, Z. J., & Liu, G. H. (2010). Monte Carlo simulation of complex cohesive fracture in random heterogeneous quasi-brittle materials: A 3D study. *International Journal of Solids and Structures, 47*, 2336-2345.

[41]. Itasca Consulting Group Inc. (2014). Users' Manual for Particle Flow Code (PFC), version 5.0. Minneapolis, Minnesota.

[42]. Potyondy, D. O., & Cundall, P. A. (2004). A bonded-particle model for rock. *International Journal of Rock Mechanics and Mining Sciences, 41*, 1329-1364.

[43]. Trent, B. C., Margolin, L. G., Cundall, P. A., & Gaffney, E. S. (1987). The micromechanics of cemented granular material. In Constitutive Laws for Engineering Materials: Theory and Applications, pp. 795-802. Amsterdam: Elsevier.

[44]. Jirasek, M., & Bazant, Z. P. (1993). Discrete element modeling of fracture and size effect in quasi-brittle materials: Analysis of sea ice. In Proceedings of the Second International Conference on Discrete Element Methods, pp. 357-368. Cambridge, MA: IESL Publications.

[45]. Donzé, F., & Magnier, S. A. (1995). Formulation of a 3-D numerical model of brittle behavior. *Geophysical Journal International, 122*, 790-802.

[46]. Bieniawski, Z. T. (1967). Mechanism of brittle fracture of rock: Part I–theory of the fracture process. *International Journal of Rock Mechanics and Mining Sciences & Geomechanics Abstracts,* 4, 395-406.

[47]. Bobet, A., & Einstein, H. H. (1998). Fracture coalescence in rock-type materials under uniaxial and biaxial compression. *International Journal of Rock Mechanics and Mining Sciences, 35,* 863-888.

[48]. Fu, J., Haeri, H., Sarfarazi, V., Noshadi, A. H., Fatehi Marji, M., & Guo, M. (2022a). Investigating the failure behavior of gypsum specimens with non-persistent vertical notch under uniaxial compression. *Strength of Materials, 54(1),* 14-32.

[49]. Fu, J., Haeri, H., Sarfarazi, V., Asgari, K., & Fatehi Marji, M. (2022b). The shear behavior of concrete-gypsum specimens containing double edge cracks under four-point loading conditions. *Theoretical and Applied Fracture Mechanics, 119*, 103361.

[50]. Kristjánsson, G. (2014). Rock bolting and pull out test on rebar bolts. PhD thesis, Norwegian University of Science and Technology, Department of Geology and Mineral Resources Engineering.

مکانیسم‌های شکست سطح اتصال بتن - پیچ: تأثیر تعداد و شکل دندانه پیچ‌سنگ

وهاب سرفرازی[۱]، لی ژو[۲،۳]، هادی حائری[۴*]، پرستو صالحی پور[۵]، علی الهی[۴]، علی معایر[۶]، محمد فاتحی مرجی[۷]

۱- بخش مهندسی معدن، دانشگاه صنعتی همدان ، ایران

۲- آزمایشگاه کلید دولتی زمین شناسی و بهره برداری از مخزن نفت و گاز، دانشگاه نفت جنوب غربی، چنگدو، ۶۱۰۵۰۰، چین

۳- آزمایشگاه کلیدی ایالتی ساخت و ساز هوشمند و عملیات سالم و تعمیر و نگهداری مهندسی زیرزمینی عمیق، کالج معماری و محیط زیست، دانشگاه سیچوان، چنگدو ۶۱۰۰۶۵، چین

۴- بخش مهندسی معدن، مجتمع آموزش عالی زرند، دانشگاه شهید باهنر کرمان، کرمان، ایران

۵-مدرسه منابع طبیعی و محیط زیست، دانشگاه ویرجینیای غربی، مورگان تاون، ویرجینیای غربی، ایالات متحده آمریکا

۶- بخش مهندسی عمران، دانشگاه آزاد اسلامی واحد شیراز، شیراز، ایران

۷-بخش مهندسی بهره برداری از معادن، دانشکده معدن و متالورژی، مؤسسه فنی و مهندسی، دانشگاه یزد، یزد، ایران

ارسال ۲۰۲۴/۰۴/۱۸، پذیرش ۲۰۲۴/۰۸/۱۵

* نویسنده مسئول مکاتبات: haerihadi@gmail.com

چکیده:

رفتار مکانیکی رابط پیچ سنگ-سنگ با در نظر گرفتن اثرات شکل فرورفتگی ها و تعداد آنها بر اساس روش المان مجزا با استفاده از کد جریان ذرات دو بعدی (PFC) به صورت عددی شبیه سازی شد. برای کالیبراسیون نمونه‌های مدل‌سازی شده با ابعاد ۱۰۰ × ۱۰۰ سانتی‌متر، از تست های معمولی و استاندارد فشاری تک محوری و مقاومت کششی برزیلی استفاده شد. مدل‌های عددی به گونه‌ای تهیه شدند که شکل و تعداد فرورفتگی‌های متفاوتی در آرایش پیچ‌های کابل در طول فرآیند تقویت سنگ درج شدند. اثرات فشار محدود ۳.۷ مگاپاسکال و بارهای مختلف شکست برشی برای آزمایش برشی پانچ نمونه‌های بتنی مدل‌سازی شد. نتایج این مطالعه نشان داد که حالت شکست غالب رابط پیچ سنگ-کابل حالت کششی بوده و شکل و تعداد فرورفتگی‌های کابل به‌طور معنی‌داری بر مقاومت و رفتار مکانیکی نمونه‌های مدل‌سازی‌شده تأثیر می‌گذارد. همچنین نشان داده شده است که ابعاد و تعداد فرورفتگی بر مقاومت برشی سطح مشترک تأثیر می گذارد.

کلمات کلیدی: مقاومت کششی، شکل نفوذ پیچ سنگ، رابط، روش المان مجزا.